

# Letters

---

## A Health Indicator of Aluminum Electrolytic Capacitors Based on Strain Sensing

Bo Yao<sup>ID</sup>, *Student Member, IEEE*, Shuai Zhao<sup>ID</sup>, *Member, IEEE*, Yichi Zhang<sup>ID</sup>, *Student Member, IEEE*, and Huai Wang<sup>ID</sup>, *Senior Member, IEEE*

**Abstract**—This letter proposes a novel health indicator for aluminum electrolytic capacitors (AECs) based on strain sensing in a nonintrusive manner. The indicator leverages the mechanism that the internal pressure of AECs gradually increases with the electrochemical reaction caused by degradation, thereby, with a change in strain. The results reveal the proposed health indicator is highly sensitive to capacitor degradation and meanwhile highly resistant to interferences. Furthermore, an end-of-life criterion for the AECs is proposed in this indicator, which is corresponding to the moment of open vent. The applicability of this indicator is verified for constant conditions, dynamic operating conditions, and overvoltage conditions. In addition, the effect of temperature is analyzed. The proposed health indicator can be used to determine the time to failure of testing samples in accelerated life testing and condition monitoring of AECs.

**Index Terms**—Aluminum electrolytic capacitors, health indicator, nonintrusive, strain sensing.

### I. INTRODUCTION

MONITORING the degradation state of aluminum electrolytic capacitors (AECs) has great significance for ensuring the reliable operation and preventing possible catastrophic failures [1]. There are two emerging demands for AECs health indicators in power electronics applications. The first is to monitor the degradation state of AECs in a low-risk and noninvasive mode. The second is to monitor the signal with wide dynamic performance and high interference immunity [2]. Most of the existing indicators have at least one of the two issues as follows.

- 1) Health indicators based on capacitance and equivalent series resistance (ESR) generally require calculations on specific voltage and current signals. In those methods, additional signals and algorithms are usually required to intrude into the original circuit structure [3]. Meanwhile, measuring voltage and current in the original circuit structure introduces noise due to electromagnetic interference

(EMI), which can lead to inaccurate estimates of the measurement results [4]. Therefore, the monitoring indicator based on capacitance and ESR has the potential risk of intruding into the original circuit and is interfered by noise [2].

- 2) The existing indicators of nonelectrical parameters for AECs still lack effective field implementation considerations. Gulbrandsen et al. [5] reported that the weight of the AEC decreases with the degradation of the capacitor, but this method requires repeated offline measurement after disassembling the AECs. The indicator based on the linear dependence between capacitance and temperature can be used in similar loading conditions, but it still has limitations due to the effects of operating conditions and ambient temperature dynamics [6].

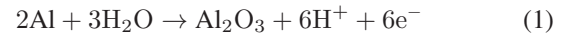
This letter proposes a novel health indicator for AECs based on strain sensing. It is inspired by the pressure inside the AEC that increases with the electrochemical reaction caused by aging and extreme conditions [7]. The aluminum case expands and ultimately opens the pressure relief vent that is attached on top of the AEC [8]. The proposed monitoring principles and experimental results reveal that the indicator based on strain sensing has the following advantages: 1) Low risk, as no intrusion into the operating circuit is required; 2) the resistive sampling signal has high sensitivity and a wide measuring range, and is highly resistant to interference; 3) the moment when the pressure relief vent opens can be used as an end-of-lifetime (EoL) criterion for AECs.

### II. FORCE SENSING MONITORING INDICATOR

#### A. Mechanism of Internal Pressure Increase for AEC

A typical AEC structure is shown in Fig. 1, consisting of the element, the aluminum case, the fixed structures, and the pressure relief vent on the top, etc. An element is constructed by using two strips of aluminum foil (anode and cathode) with paper interleaved [8].

Due to long-term degradation or extreme conditions, such as high temperature, overvoltage, and excess ripple current, a sudden increase in hydrogen ion  $H^+$  is generated [8]



where  $H^+$  indicates Hydrogen ion, which combines with electrons  $e^-$  to produce hydrogen gas  $H_2$ .

Manuscript received 11 January 2023; revised 24 February 2023; accepted 13 March 2023. Date of publication 29 March 2023; date of current version 19 May 2023. (*Corresponding author: Shuai Zhao*.)

The authors are with the Department of Energy, Aalborg University, 9220 Aalborg, Denmark (e-mail: ybo@energy.aau.dk; szh@energy.aau.dk; yzhang@energy.aau.dk; hwa@et.aau.dk).

Color versions of one or more figures in this article are available at <https://doi.org/10.1109/TPEL.2023.3263125>.

Digital Object Identifier 10.1109/TPEL.2023.3263125

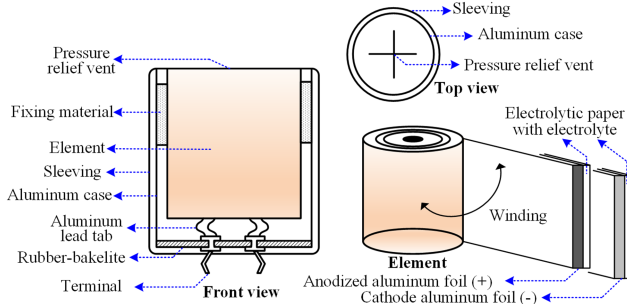


Fig. 1. Construction of aluminum electrolytic capacitors.

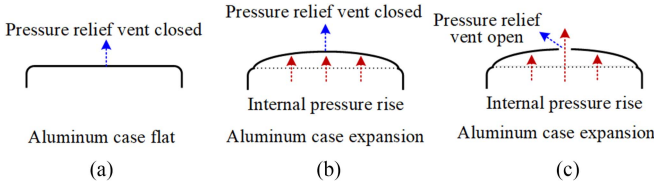


Fig. 2. Internal pressure of aluminum electrolytic capacitors and operation principle of pressure relief vent. (a) Initial condition. (b) Progressive aging condition. (c) Reach the critical point condition.

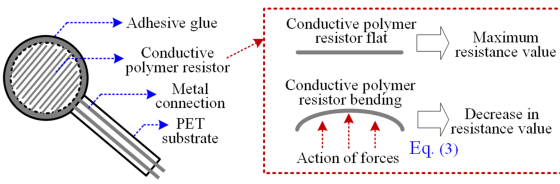
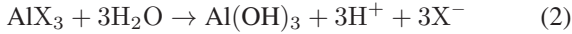


Fig. 3. Architecture and operation principle of the strain sensor.

When a halide substance seeps into the AECs, the following electrochemical reaction also occurs [8]:



where  $\text{X}^-$  indicates halogen ions ( $\text{Cl}^-$ ,  $\text{F}^-$ ,  $\text{Br}^-$ ).

In Fig. 2, the aluminum case at the top is initially flat and the pressure relief vent is closed in the initial condition. When the chemical reaction is repeated to produce gas with long-term degradation or extreme conditions, the internal pressure rises, causing the aluminum case at the top to expand outward and the pressure relief vent to start operating. Finally, when the internal pressure reaches a critical point, the pressure relief vent is opened and the resulting gas is discharged at the top.

### B. Principle of the Strain Sensor

In Fig. 3, a typical strain sensor consists of the conductive polymer resistance, the adhesive spacer, the metal connection, and the plastic substrate [9]. Following the application of force to the surface of the strain sensor, the conductive polymer resistance is deformed, resulting in a decrease in resistance [10].

The corresponding relationship between resistance and force for one type of the strain sensor is given in Fig. 4 [9], which follows:

$$R = 10^A \times F^B \quad (3)$$

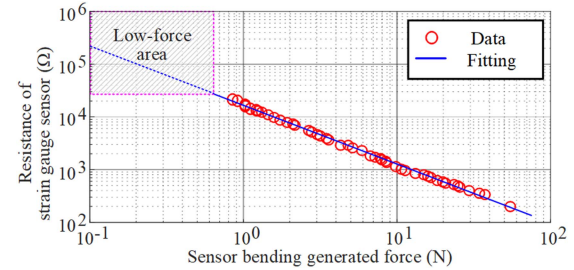


Fig. 4. Relationship between resistance and force for selected strain sensors.

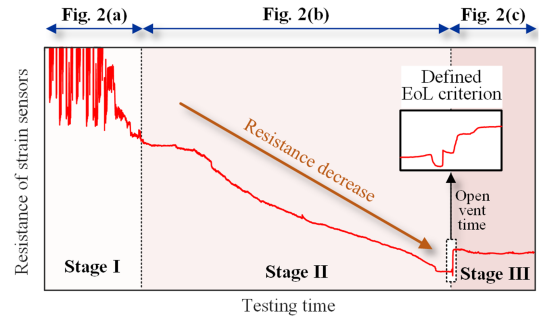


Fig. 5. Illustration of the typical patterns of the proposed health indicator.

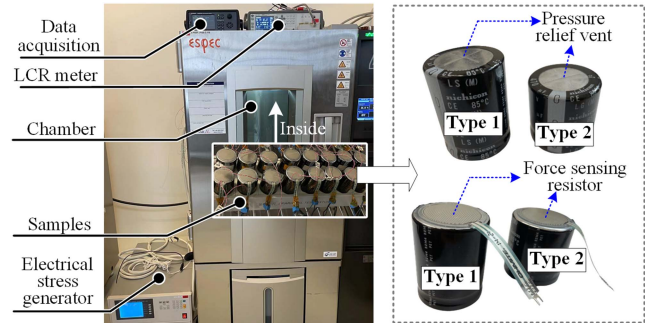


Fig. 6. Photo of the experiment platform and samples. (Two series AECs: Type 1 has a longer life expectancy - LLS2W471MELC [11] and Type 2 has a smaller size - LLG2W471MELC35 [12]).

TABLE I  
PARAMETERS OF THE CAPACITOR UNDER TEST

Rate capacitance	470 $\mu\text{F}$		
Rate dc voltage	450 V		
Rate ambient temperature	85 °C		
Rate rms current (120Hz)	Case 1	Case 2	Case 3
Test dc voltage	450 V	450 V	495 V
Test ambient temperature	95 °C	75~95 °C	85 °C
Test rms current (120Hz)	2.68 A	1.34~2.68 A	2.68 A
Signal acquisition frequency	0.1 Hz		

where  $F$  and  $R$  are the force and resistance for the strain sensors, respectively. A and B denote two coefficients of the strain sensors. For the specific strain sensor,  $A = 4.219$  and  $B = -1.114$ .

### C. Proposed Monitoring Indicator

According to the failure mode for the AECs [13], the failures caused by the application of AECs (long-term aging, excessive

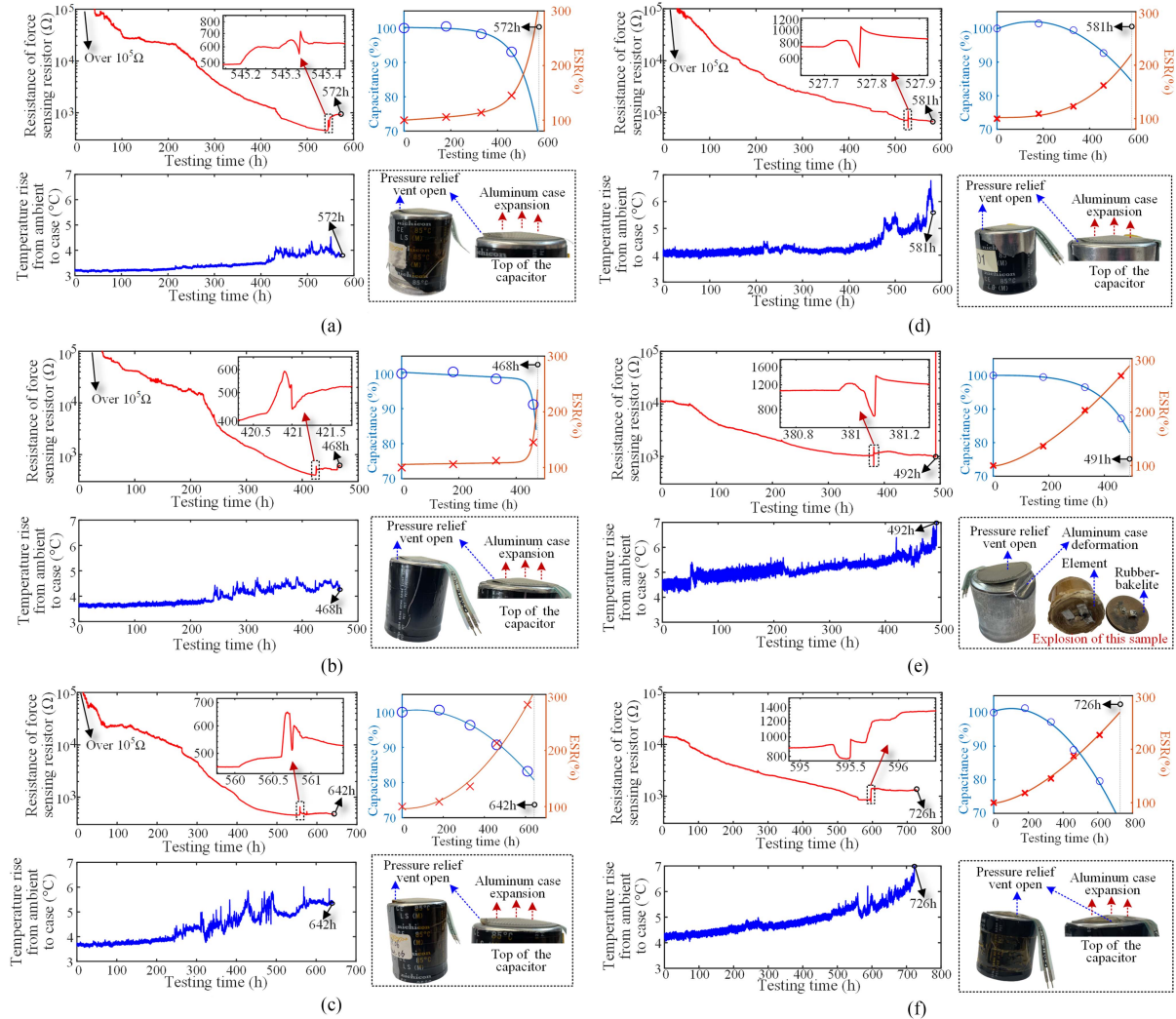


Fig. 7. Case 1: Accelerated degradation results under constant ripple current and ambient temperature. In the results of each sample, the top left indicates strain sensor, the bottom left indicates thermal stress, the top right indicates capacitance and ESR in off-line measurement at 25 °C and 120 Hz, and the bottom right indicates failure behavior. (a) Sample 1 results (Type 1). (b) Sample 2 results (Type 1). (c) Sample 3 results (Type 1). (d) Sample 4 results (Type 2). (e) Sample 5 results (Type 2). (f) Sample 6 results (Type 2).

electrical, and thermal stresses, etc.) result in a rise in internal pressure, ultimately leading to the opening of the pressure relief vent. Therefore, the resistance of the strain sensor can be used as the health indicator for AECs, as shown in Fig. 5, which is divided into three stages.

**Stage I:** The AEC is in a state where the top aluminum case is flat [Fig. 2(a)]. At this stage, the strain sensor is in a low-force area of Fig. 4, and its sensitivity to external shape variation is high.

**Stage II:** The internal pressure of the capacitor increases, causing the top aluminum case to expand [Fig. 2(b)]. During this stage, the AEC undergoes aging, causing the strain sensor to bend and the resistance to gradually decrease.

**Stage III:** After the safety valve of the capacitor is opened [Fig. 2(c)], the resistance of the strain sensor changes instantly, and then the AEC reaches actual time to failure.

The boundary between Stage II and Stage III is the presence of open vents. Similar to the health indicators based on capacitance and ESR, an EoL criterion can be defined based on the strain

sensor output resistance. The proposed EoL criterion as follows considers both the resistance value and its changing rate:

$$\begin{cases} R \leq R|_{\text{Threshold}} \\ \frac{dR}{dt} \geq \frac{dR}{dt}|_{\text{Threshold}} \end{cases} \quad (4)$$

where  $R|_{\text{Threshold}}$  and  $\frac{dR}{dt}|_{\text{Threshold}}$  are resistance threshold and resistance change rate threshold, respectively.

### III. EXPERIMENTAL SETUP

The experimental platform is shown in Fig. 6, and its main parameters are shown in Table I, in which three testing cases are set. The electrical stress generator is used to simulate the electrical stress generated by the converter (both dc voltage and ripple current/voltage) to the AECs [14]. Strain sensors are attached to the top of each sample on the surface [15]. In the degradation testing Case 1, the dc test voltage and ripple test current are kept at rated values and the test temperature is set ten degrees higher than the rated ambient temperature. In the dynamic condition testing Case 2, the dc test voltage is kept at

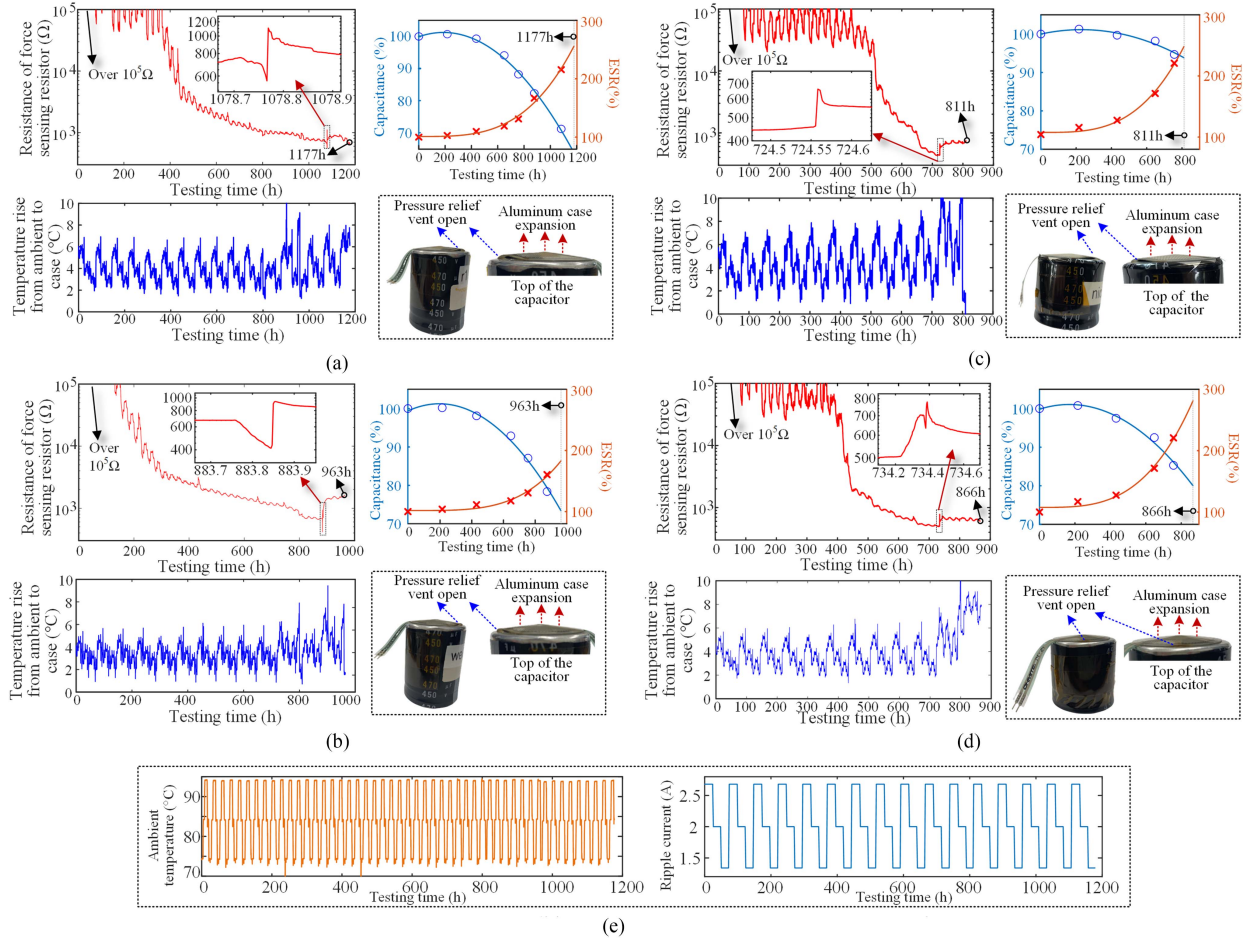


Fig. 8. Case 2: Testing results of the dynamic condition. In the results, the representation of each sample is consistent with Case 1. (a) Sample 1 results (Type 1). (b) Sample 2 results (Type 1). (c) Sample 3 results (Type 2). (d) Sample 4 results (Type 2). (e) Dynamic operation of ambient temerature and ripple current in case 2.

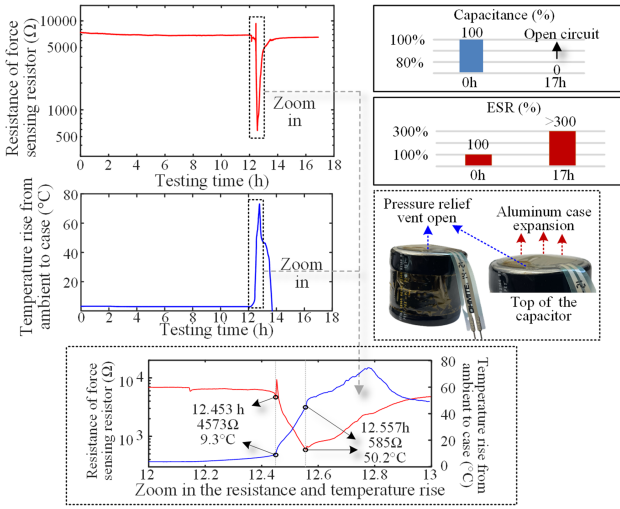


Fig. 9. Case 3: Testing results of the overvoltage condition for strain sensor, thermal stress, capacitance/ESR, and failure behavior.

the rated value, and the ripple test current (1.34–2.68 A) and test temperature (75–95  $^{\circ}\text{C}$ ) are set as the dynamic value. In the overvoltage extreme testing Case 3, the dc test voltage is set

at 1.1 times the rated value, and the ripple test current and test temperature are kept at rated values.

#### IV. TESTING RESULTS

##### A. Case 1: Degradation Testing Results

The accelerated degradation testing continues until each sample undergoes an open circuit or short-circuit catastrophic failure. During the initial stage, since the internal pressure of the AECs has not risen, the top of the aluminum case is flat, as shown in the state of Fig. 2(a). At this time, the strain sensor is in a low-force area of Fig. 4, and its sensitivity to external shape variation is high (Stage I in Fig. 5). For effective illustration purposes, the vertical coordinate is limited to 100 k $\Omega$ . From the six samples in Fig. 7, the resistance of strain sensors drops from the initial 10 k $\Omega$   $\sim$  100 k $\Omega$  to less than 1 k $\Omega$  at the time of opened vent. This result also indicates that the aging of the capacitor is a nonlinear process, with a slow aging rate at the beginning (such as Sample 1 at 0–420 h and Sample 2 at 0–250 h). When approaching the EoL, this aging speed is accelerated. Compared to the results of temperature rise from case to ambient by the thermocouples, the results of the strain sensor decrease exponentially in value with test time. It shows

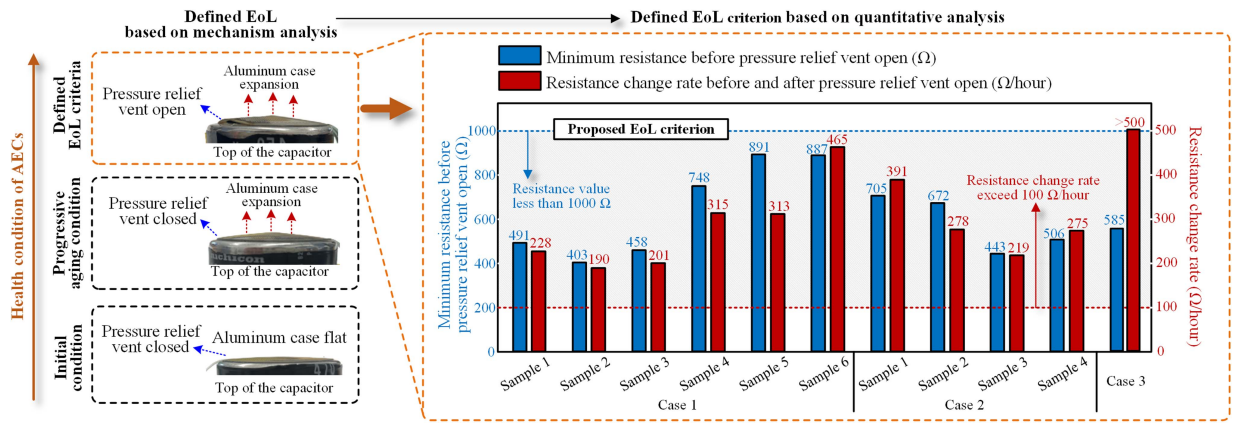


Fig. 10. Strain sensor output resistances at the presence of open vent of the testing samples. (The corresponding EoL criterion is when resistance reduces 1000  $\Omega$  and its changing rate reaches 100  $\Omega/\text{hour}$ ).

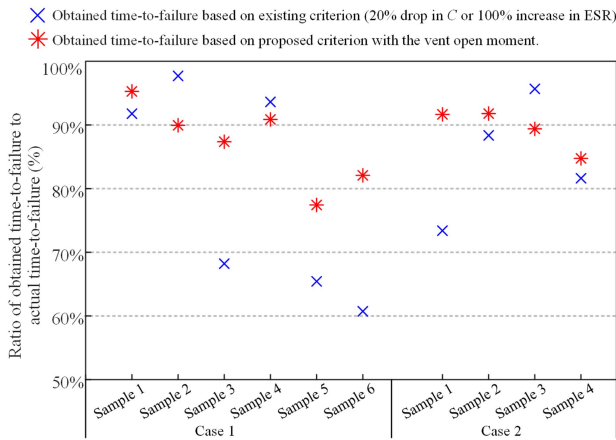


Fig. 11. Obtained time to failure of the testing samples based on the existing EoL criterion and the proposed one, with respect to the actual time to failure. Note: 1) 100% represents the actual time to failure, and 2) with  $C$  and ESR-based EoL criterion, the time to failure depends on either  $C$  or ESR meets the criteria first).

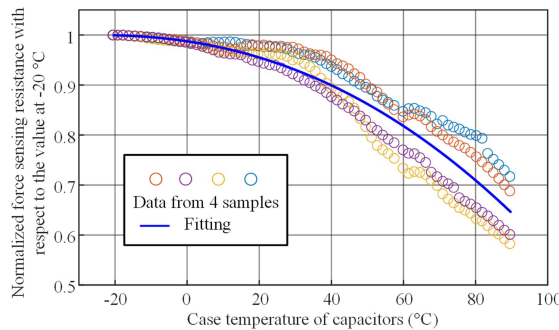


Fig. 12. The measured temperature dependence of the output resistance of the selected strain sensor.

that the strain sensor has high sensitivity, a wide measuring range, and better immunity to interference.

### B. Case 2: Dynamic Condition Testing Results

Fig. 8 shows the test results with the dynamic condition of ambient temperature and ripple current. In the early stage

of the testing process, the strain-sensing resistance is greatly affected by the operation condition of temperature dynamics, which corresponds to the low-force area in Fig. 4 and Stage I in Fig. 5. With the AECs aging, the force-strain resistance is negligibly affected by temperature dynamics at low resistance stages (below 10 k $\Omega$ ). The strain sensor results have a wider dynamic range and immunity to interference than the results from temperature rise. Therefore, the proposed monitoring indicator is still valid under dynamic operation conditions with different ambient temperature and different ripple current.

### C. Case 3: Extreme Voltage Condition Testing

Fig. 9 shows the test results for the overvoltage condition, where the AEC fails rapidly. It can be seen that the resistance of the strain sensor drops rapidly from 4573  $\Omega$  at 12.45 h to 585  $\Omega$  at 12.56 h. Its resistance change corresponds to the change in AEC temperature rise. Therefore, the proposed monitoring indicator is still valid under extreme conditions such as overvoltage.

## V. DISCUSSION

### A. Proposed EoL Criterion

In Figs. 7–9, an event is observed where there is an abrupt change in the resistance of the strain sensor for each sample. This sudden change corresponds to the state of the pressure relief vent from normal operation to opening, as depicted in Figs. 2 and 5. The change in resistance of the strain sensor when the pressure relief vent opens is analyzed with eleven samples from three cases, thereby providing a quantitative definition of the physical-failure-based EoL criterion, as shown in Fig. 10. It can be defined that the resistance of the strain gauge is lower than 1 k $\Omega$ , with a resistance change rate exceeding 100  $\Omega/\text{hour}$ .

The proposed EoL criterion and existing capacitance/ESR-based EoL criterion are compared in Fig. 11. First, the time of catastrophic open circuit or short-circuit failure is defined as the actual time to failure. The time based on EoL criterion is defined as the obtained time to failure. Based on the existing criterion, the obtained time to failure of the samples is between 60% and 100% of the actual time to failure. The obtained time

to failure with the proposed EoL criterion is between 75% and 100% of the actual time to failure. Compared to the existing EoL criterion, the proposed EoL criterion achieves smaller variances with respect to the actual time to failure at the time at the presence of opened vent. Furthermore, the failure performance of Sample 5 in Case 1 highlights the risk of explosion if the capacitor is further tested after the vent has opened. Therefore, the proposed EoL criterion is reasonable based on the results of the analysis of testing samples.

### B. Temperature Effects of Force Sensing Resistors

After normalizing the resistance of sensing resistors, the corresponding relationship between temperature and resistance for the strain sensor with the four samples is given in Fig. 12, which can be numerically fitted as

$$R = R_0 \left[ 1 - 9.21 \times 10^{-6} \times (T_{\text{case}} - T_0)^{2.25} \right] \quad (5)$$

where  $R$  and  $T_{\text{case}}$  are the strain-sensing resistance ( $\Omega$ ) and case temperature ( $^{\circ}\text{C}$ ), respectively.  $R_0$  and  $T_0$  indicate the reference of strain-sensing resistance and case temperature ( $-20\ ^{\circ}\text{C}$ ), respectively.

The maximum effect of temperature sensitivity on resistance values is 42% (from  $-20\ ^{\circ}\text{C}$  to  $90\ ^{\circ}\text{C}$ ). The temperature effect of the resistance change is negligible, compared to the change in resistance of at least tenfold drop during aging in Figs. 7 and 8.

### C. Possible Application of the Proposed Health Indicator

- 1) *Offline Applications:* The proposed health indicator can be used to determine the EoL of capacitor testing samples during accelerated life testing.
- 2) *Online Applications:* For the condition monitoring of both single capacitor or banks with multiple capacitors. A strain sensor can be attached on the surface of each individual AEC. The thickness of strain sensors is typically in the range of submillimeter, e.g., it is 0.425 mm for the testing samples discussed in the case study [15], which has negligible size. Moreover, strain sensors typically operate in the temperature range of  $-20\ ^{\circ}\text{C}$  to  $85\ ^{\circ}\text{C}$  [15], which can meet a wide range of capacitor applications.

## VI. CONCLUSION

This letter proposes a health indicator for AECs based on the output resistance of strain sensors. The resistance drops with the increase of the internal pressure of AECs due to electrochemical related degradation. Nevertheless, at the time when the AEC vent is opened, the resistance starts to increase fast due to the AEC internal pressure reducing abruptly. Therefore, there are distinctive patterns of the resistance changes (see Fig. 5). Accordingly, an EoL criterion is also proposed based on both the resistance value and its change rate. Eleven capacitor samples have been tested under three cases of constant ambient temperature and

ripple current, dynamic ambient temperature and ripple current, and overvoltage conditions. The results reveal that the proposed health indicator and EoL criterion can effectively obtain the time to failure of the testing samples. Compared to the existing EoL criterion based on capacitance  $C$  and ESR, the proposed EoL criterion achieves smaller variances with respect to the actual time to failure at the time of opened vent (see Fig. 11). Moreover, the proposed health indicator can be obtained based on a noninvasive way since it does not require capacitor electrical signals, making it promising for both offline and online applications, such as capacitor accelerated life test and condition monitoring. It should be noted that the proposed health indicator is limited to capacitors (or also other type of electronic components if applicable) which have internal pressure increase due to certain degradation mechanism(s).

## REFERENCES

- [1] H. Wang and F. Blaabjerg, "Reliability of capacitors for DC-link applications in power electronic converters—An overview," *IEEE Trans. Ind. Appl.*, vol. 50, no. 5, pp. 3569–3578, Sep./Oct. 2014.
- [2] Z. Zhao, P. Davari, W. Lu, H. Wang, and F. Blaabjerg, "An overview of condition monitoring techniques for capacitors in DC-link applications," *IEEE Trans. Power Electron.*, vol. 36, no. 4, pp. 3692–3716, Apr. 2021.
- [3] Y. Wu and X. Du, "A VEN condition monitoring method of DC-link capacitors for power converters," *IEEE Trans. Ind. Electron.*, vol. 66, no. 2, pp. 1296–1306, Feb. 2019.
- [4] C. Liu, F. Deng, Q. Yu, Y. Wang, F. Blaabjerg, and X. Cai, "Submodule capacitance monitoring strategy for phase-shifted carrier pulselength-modulation-based modular multilevel converters," *IEEE Trans. Ind. Electron.*, vol. 68, no. 9, pp. 8753–8767, Sep. 2021.
- [5] S. Gulbrandsen, J. Arnold, N. Kirsch, and G. Caswell, "A new method for testing electrolytic capacitors to compare life expectancy," in *Proc. IMAPS Device Packag. Conf.*, 2014, pp. 1759–1786.
- [6] Q. Luo, B. Luo, Y. Zhu, H. Wang, Q. Wang, and G. Zhu, "Condition monitoring of DC-link capacitors by estimating capacitance and real-time core temperature," in *Proc. IEEE 13th Int. Symp. Power Electron. Distrib. Gener. Syst.*, 2022, pp. 1–5.
- [7] Z. Dou, X. Rong, B. Alfonso, Q. Javaid, and P. Cynthia, "Performance of aluminum electrolytic capacitors and influence of aluminum cathode foils," in *Proc. CARTS Europe*, 2010, pp. 1–17.
- [8] "General descriptions of aluminum electrolytic capacitors," Nichicon, Kyoto, Japan, 2019. [Online]. Available: <https://www.nichicon.co.jp/english/products/pdf/aluminum.pdf>
- [9] "FSR integration guide and evaluation parts catalog," SparkFun Electronics, Boulder, CO, USA, 2018. [Online]. Available: <https://www.sparkfun.com/datasheets/Sensors/Pressure/fsrguide.pdf>
- [10] Y. Wei and Q. Xu, "An overview of micro-force sensing techniques," *Sensors Actuators A: Phys.*, vol. 234, pp. 359–374, 2015.
- [11] "LS series of aluminum electrolytic capacitors," Nichicon Corporation, Kyoto, Japan, 2011. [Online]. Available: <https://www.nichicon.co.jp/english/products/pdfs/e-ls.pdf>
- [12] "LLG series of aluminum electrolytic capacitors," Nichicon Corporation, Kyoto, Japan, 2015. [Online]. Available: <https://www.nichicon.co.jp/english/products/pdfs/e-llg.pdf>
- [13] "Technical note - Judicious use of aluminum electrolytic capacitors," Nippon Chemi-Con Corporation, Tokyo, Japan, 2019. [Online]. Available: <https://www.chemi-con.co.jp/products/relatedfiles/capacitor/catalog/al-technote-e.pdf>
- [14] "Ripple current tester model 11800/11801/11810," Chroma ATE Inc., Taiwan, 2019. [Online]. Available: [http://www.chromaate.com/product/11800\\_11801\\_11810\\_Ripple\\_Current\\_Tester.htm](http://www.chromaate.com/product/11800_11801_11810_Ripple_Current_Tester.htm)
- [15] "FSR series of force sensing resistor," Ohmite Manufacturing Company, Warrenville, IL, USA, 2019. [Online]. Available: <https://docs.rs-online.com/86be/A70000007054163.pdf>